Journal of Orthopaedic Translation 24 (2020) 39–45

Contents lists available at ScienceDirect

Journal of Orthopaedic Translation

journal homepage: www.journals.elsevier.com/journal-of-orthopaedic-translation

ORIGINAL ARTICLE

# Differences in subchondral trabecular bone microstructure and finite element analysis-based biomechanical properties between osteoporosis and osteoarthritis

Zihao He [a], Linyang Chu [a,b,1], Xuqiang Liu [c], Xuequan Han [a], Kai Zhang [a], Mengning Yan [a], Xiaofeng Li [c,**], Zhifeng Yu [a,*]

[a] Shanghai Key Laboratory of Orthopedic Implant, Department of Orthopedics, Shanghai Ninth People's Hospital, Shanghai Jiao Tong University School of Medicine, Shanghai, 200011, China
[b] Department of Orthopaedics, Shanghai Jiao Tong University Affiliated Sixth People's Hospital, Shanghai, 200011, China
[c] Department of Orthopedics, The First Affiliated Hospital of Nanchang University, The Artificial Joint Engineering and Technology Research Center of Jiangxi Province, Nanchang, Jiangxi, China

ARTICLE INFO

*Keywords:*
Finite element analysis
Individual trabecular segmentation
Mechanical property
Osteoarthritis
Osteoporosis

SUMMARY

*Background/Objective:* The microstructure of the subchondral trabecular bone, including the composition and distribution of plates and rods, has an important influence on the disease progression and mechanical properties of osteoarthritis (OA) and osteoporosis (OP). We aimed to determine whether differences in plates and rods influence the variations in the quantities and qualities of the subchondral trabecular bone between OA and OP.
*Materials and methods:* Thirty-eight femoral head samples [OA, n = 13; OP, n = 17; normal control (NC), n = 8] were collected from male patients undergoing total hip arthroplasty. They were scanned using microcomputed tomography, and subchondral trabecular structures were analysed using individual trabecular segmentation. Micro-finite element analysis (μFEA) was applied to assess the mechanical property of the trabecular bone. Cartilage changes were evaluated by using histological assessment. Analysis of variance was used to compare intergroup differences in structural and mechanical properties and cartilage degradation. Pearson analysis was used to evaluate the relationship between the trabecula microstructure and biomechanical properties.
*Results:* Compared with the OP and NC group, there was serious cartilage damage in the OA group. With respect to the microstructure results, the OA group had the highest plate and rod trabecular microstructures including number and junction density among the three groups. For the mechanical properties detected via μFEA, the OA group had higher stiffness and failure load than did the OP group. Pearson analysis revealed that compared with OP, OA had a higher number of microstructure parameters (e.g., rod bone volume fraction and rod trabecular number) that were positively correlated with its mechanical property.
*Conclusions:* Compared with OP, the OA subchondral bone has both increased plate and rod microarchitecture and has more microstructures positively related with its mechanical property. These differences may help explain the variation in mechanical properties between these bone diseases.
*The translational potential of this article:* Our findings suggested that changes in the plates and rods of the subchondral trabecular bone play a critical role in OA and OP progression and that the improvement of the subchondral trabecular bone may be a promising treatment approach.

## Introduction

Osteoarthritis (OA) is a chronic skeletal disease characterised by a potential loss and fragmentation of the joint cartilage with other joint changes including osteophyte formation and subchondral bone changes [1,2]. Meanwhile, osteoporosis (OP) is a metabolic bone disease

* Corresponding author.
** Corresponding author.
*E-mail addresses:* doctorli000@163.com (X. Li), zfyu@outlook.com (Z. Yu).
[1] Co-first authors

https://doi.org/10.1016/j.jot.2020.05.006
Received 29 February 2020; Received in revised form 12 May 2020; Accepted 21 May 2020
Available online 2 June 2020

characterised by low bone mass, which may damage the skeletal structure and cause fractures [3,4]. OA and OP commonly occur in the elderly population and are the leading causes of disability that significantly affects the individual quality of life. However, evidence suggested that these diseases rarely occur concurrently [5–10], which implies a difference in the underlying pathological process between the two diseases. The subchondral bone, located in the cancellous bone layer below the cartilage within the joint [11], carries most of the mechanical force transmitted by the joint [12,13]. Both OA and OP can affect the structure of the subchondral bone [14]. Subchondral bone sclerosis is one of the hallmarks of advanced OA [15,16] and may cause cartilage lesions [17]. Meanwhile, decreased subchondral bone volume and increased fragility are the hallmarks of OP. Therefore, a more detailed comparison of the subchondral bones between OA and OP may increase our understanding of the pathological differences between them and help with their diagnosis.

Accordingly, some studies have focused on the subchondral bone changes associated with OA and OP. By comparing the microcomputed tomography (μCT)–based structural differences and mechanical properties of the subchondral bone in postmenopausal women [18,19]. They found that the better resistance to fatigue damage seen in OA patients may be attributed to the increases in bone mass and plate-like structures. Structural differences can be caused by differences in bone remodelling. Postmenopausal OP patients showed increased bone resorption that led to the loss of bone mass [20,21], while OA may contribute to bone mass and bone strength through bone formation by osteoblasts [22]. While these structural changes of the subchondral bone are interesting, their research did not rule out the possibility of OP in the OA patients via dual-energy X-ray absorptiometry (DXA) [18,19], even if the two diseases are less likely to appear simultaneously. In addition, they only analysed the conventional μCT structure, which does not show detailed properties of the trabecular rod and plates, including number density, thickness, and orientation.

However, analysing the subtle differences in the structure and mechanical properties of the subchondral trabecular bone can be helpful to further understand the pathophysiology of bone diseases. The individual trabecula segmentation (ITS)–based morphological analysis technique divides the topographic orientation of cancellous bone elements into rod and plate parts. This technique can detect subtle differences in the trabecular plate and rod microstructure and help predict the mechanical properties of the cancellous bone based on the standard morphological parameters [23,24].

This study aimed to investigate the structural differences of the two diseases and their relationship with mechanical properties and cartilage damage. Towards this goal, we conducted a more detailed assessment of the subchondral bone microarchitecture by using the ITS technique. We hypothesised that the subchondral trabecular bone plate and rod changes may contribute differently to OA and OP mechanical properties.

## Materials and Methods

### *Subjects, diagnoses, assessment of bone mineral density, and specimen preparation*

This cross-sectional study was approved by the local ethical review board (IRB reference number: 2018-179-T137). All patients provided written informed consent. The subjects were patients diagnosed with hip fractures or primary hip OA based on radiographic and clinical diagnostic criteria and underwent total hip replacement surgery at our institution. OA and OP were diagnosed by the same experienced doctor according to the American College of Rheumatology criteria [25] and the World Health Organization protocol, respectively. Briefly, the diagnosis of OP was made when the T score was less than or equal to −2.5 (T-score ≤ -2.5) [4]. Areal bone mineral density of the lumbar spine (L1–L4) and hip was measured using DXA (Hologic Discovery A; Hologic, Walton, MA, USA). We excluded patients with thyrotoxicosis, metabolic diseases of the liver and kidney, or malignancies as well as those who received glucocorticoids and OP drugs during the previous year. Patients with any evidence of OP on DXA were excluded from the OA group, and patients with any evidence of OA were excluded from the OP and NC group. In total, 38 patients were included in the study. Of them, 13 patients who had OA, 17 patients who had fractured femoral neck with OP, and 8 patients who had traumatic fractured femoral neck with normal bone mineral density were categorised into the OA group, OP group, and the normal control (NC) group. All femoral head specimens were fixed in 4% formalin for 48 h and rinsed overnight before further study.

### *μCT scan and ITS analysis*

Whole femur head specimens were scanned using μCT (μCT 80; Scanco Medical AG, Switzerland). Previous studies showed that the axes of the specimens were perpendicular to the articular surface [14,26]. Thus, to avoid disturbing regional differences, only the most heavily loaded area, i.e. the superior part, was selected for the measurement. The scanning setting was 70 kVp, 114 μA, and a 300-ms integration time with an isotropic 36-μm voxel size. As the volume of interest in the principal load-bearing region, virtual cylindrical biopsies (Ø 5.4 mm, L 5.4 mm) determined using the semiautomatic contouring method were extracted from the reconstructed 3D image (cubic sub-volume; Fig. 1). The volume of interest was determined using the semiautomatic contouring method. The scan generated a series of planar transverse grayscale images, and all images were segmented using a low-pass filter to remove noise using the same threshold to determine the bone phase. Image Processing Language v4.29d software (Scanco Medical AG, Switzerland) was used to process the total bone microstructure. The conventional μCT parameters including bone volume fraction (BV/TV, %), trabecular number (Tb.N, 1/mm), trabecular thickness (Tb.Th, μm), trabecular separation (Tb.Sp, $mm^2$), and junction density (Junc.D, $1/mm^3$) were calculated. A model based on the type of the structure was used to measure the structure model index (SMI). An ideal segmented plate structural model has an SMI value of 0, whereas a segmented cylindrical rod structural model has an SMI value of 3.

All trabecular bone sub-volumes were subjected to ITS-based morphological analyses [23,24]. A complete volumetric decomposition technique was applied to segment the trabecular network into individual plates and rods. Briefly, using digital topologic analysis (DTA), the skeletal network of the bone trabecular network was transformed into a representative skeleton made of surfaces and curves, and the rod and

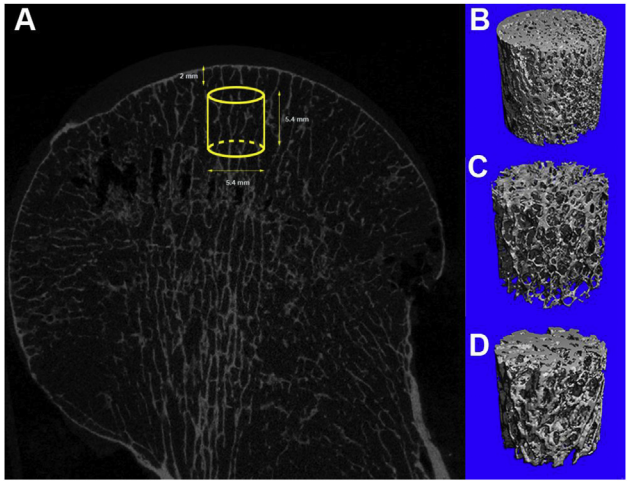


**Fig. 1.** Micro-CT view of the femoral head specimens (A) The location of virtual cylindrical biopsies extracted from the image (yellow cubic subvolume of interest) (B–D) The reconstructed 3D image of the OA (B), OP (C), and NC (D) groups. (For interpretation of the references to colour in this figure legend, the reader is referred to the Web version of this article.)

**Table 1**
Anthropometric, T value, and Bone Density of the OA, OP and NC groups.

| Characteristics | OA, mean ± SD | OP, mean ± SD | NC, mean ± SD | ANOVA p Value |
|---|---|---|---|---|
| N | 13 | 17 | 8 | |
| Gender (Female/ Male) | 10/3 | 13/4 | 4/4 | |
| age (years) | 52.31 ± 13.39 | 75.71 ± 9.82 | 65.25 ± 23.3 | <0.001* |
| Height (cm) | 163.38 ± 7.57 | 160.12 ± 6.18 | 164.63 ± 6.76 | 0.311 |
| Weight (kg) | 63.23 ± 11.1[a] | 54.24 ± 9.31[b] | 65.13 ± 3.83 | <0.001* |
| Body Mass Index (kg/ $m^2$) | 23.55 ± 2.53 | 21.14 ± 3.35 | 24.13 ± 2.37 | 0.029 |
| Femur T value | −0.53 ± 1.07 | −2.26 ± 1.07[b] | −1.11 ± 0.86 | <0.001* |
| Lumbar T value | −0.69 ± 0.97 | −3.55 ± 1.12[b] | −0.71 ± 1.41 | <0.001* |
| Femur BMD (g/ $cm^2$) | 0.89 ± 0.15 | 0.6 ± 0.14[b] | 0.79 ± 0.08 | <0.001* |
| Lumbar BMD ($g/cm^2$) | 0.91 ± 0.1 | 0.59 ± 0.12[b] | 0.91 ± 0.14 | <0.001* |
| OARSI score | 14.38 ± 3.97[a] | 4.53 ± 2.62[b] | 3.25 ± 1.58 | <0.001* |

Values represent mean ± SD.
BMD = bone mineral density; NC = normal control; OA = osteoarthritis; OP = osteoporosis.
*p < 0.05 between OA and OP group.
[a] p<0.05 between OA and NC group.
[b] p < 0.05 between OP and NC group.

plate shapes of the trabecular microstructure were maintained. Each skeletal voxel was uniquely classified by the DTA classification [23,27]. Utilizing the iterative reconstruction measure as previously reported, each skeletal voxel was classified as an individual type of either plate or rod [23]. Based on the evaluations for each individual bone trabecular plate or rod, a series of ITS-based morphological parameters were calculated at the junctions of the plate and rod trabeculae, including the axial bone volume fraction (aBV/TV, %), plate and rod bone volume fraction (pBV/TV and rBV/TV, %), plate and rod trabecular number (pTb.N and rTb.N, 1/mm), plate and rod trabecular thickness (pTb.Th and rTb.Th, μm), plate trabecular surface area (pTb.S, $mm^2$), rod trabecular length (rTb.l, mm), junction density between rod and rod (R–R Junc. D, $1/mm^3$), rod and plate (R–P Junc. D, $1/mm^3$), and plate and plate (P–P Junc. D; $1/mm^3$). The definition of these ITS-based microstructural parameters and detailed methods of their applied techniques were reported previously [23,28].

*Mechanical tests and micro-finite element analysis*

Scanco Medical Finite Element Software 1.06 (Scanco Medical AG, Bassersdorf, Switzerland) was used for micro-finite element analysis (μFEA) to simulate the axial compression tests for each trabecular bone in the longitudinal directions. Trabecular bone tissues were modelled as an isotropic linear elastic material with a Young's modulus of 15 GPa and a Poisson's ratio of 0.3 [29–31]. For each bone segment model, uniaxial compression tests were performed for the μFEA analysis to calculate the reaction force under a displacement equal to 1% of the bone segment height along the axial direction. This allowed us to determine bone stiffness and failure load values, which represented the mechanical properties. Bone stiffness, defined as reaction force divided by the applied displacement, characterises the mechanical competence of the subchondral trabecular compartment. The percentage of load at subchondral bone of the trabecular segment was calculated as the reaction force at the trabecular bone surface divided by the total reaction force, based on a previous study [32].

*Cartilage assessment via histology*

Specimens were fixed in 4% buffered formalin for 48 h, and the cartilage regions were collected. Then, the cartilages were decalcified in 10% ethylenediaminetetraacetic acid (pH 7.4) for 21 days and embedded

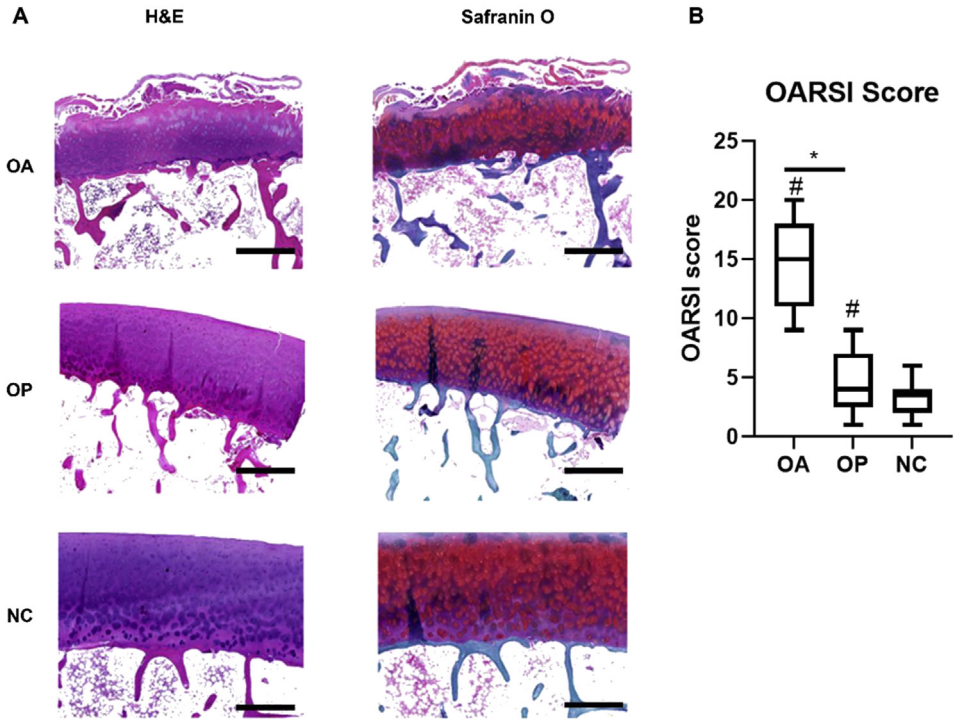


**Fig. 2.** Articular cartilage evaluation and its association with the subchondral bone microstructure (A) Histological analysis of cartilage damage in the OA, OP, and NC groups (B) The Osteoarthritis Research Society International (OARSI) scores of the OA, OP, and NC groups. * Significant difference between OA and OP group ($p < 0.05$). # Significant difference compared with the NC group ($p < 0.05$). Scale bars = 200 μm.

**Table 2**
Comparsion of microarchitecture in the OA, OP and NC groups.

| Microstructure | OA, mean ± SD | OP, mean ± SD | NC, mean ± SD | p Value |
|---|---|---|---|---|
| **Standard micro-CT** | | | | |
| BV/TV (%) | 29.85 ± 13.37 | 15.65 ± 6.13 | 22.64 ± 5.07 | 0.001* |
| Tb.N (1/mm) | 2.47 ± 1.08[a] | 1.26 ± 0.33 | 1.53 ± 0.29 | <0.001* |
| Tb.Th (mm) | 0.19 ± 0.03 | 0.17 ± 0.03 | 0.19 ± 0.03 | 0.147 |
| Tb.Sp (mm) | 0.53 ± 0.27 | 0.86 ± 0.2 | 0.68 ± 0.1 | 0.001* |
| SMI | 0.87 ± 0.91 | 1.52 ± 0.81 | 0.98 ± 0.51 | 0.079 |
| Conn.D (1/mm3) | 16.05 ± 9.72[a] | 7.14 ± 3.94 | 7.7 ± 3.92 | 0.002* |
| **ITS-based micro-CT** | | | | |
| pBV/TV (%) | 22.72 ± 9.46 | 12.66 ± 6 | 17.76 ± 6.08 | 0.007 |
| rBV/TV (%) | 7.12 ± 4.61 | 3 ± 1.65 | 4.88 ± 2.26 | 0.003* |
| aBV/TV (%) | 14.66 ± 5.97 | 8.6 ± 4.27 | 12.03 ± 3.88 | 0.004* |
| pBV/BV (%) | 77.26 ± 6.11 | 77.89 ± 15.41 | 77.05 ± 12.92 | 0.217 |
| rBV/BV (%) | 22.75 ± 6.11 | 22.11 ± 15.41 | 22.95 ± 12.92 | 0.224 |
| pTb.N (1/mm) | 3.06 ± 0.41[a] | 2.47 ± 0.37 | 2.41 ± 0.53 | 0.001* |
| rTb.N (1/mm) | 2.82 ± 0.48[a] | 2.23 ± 0.4 | 2.1 ± 0.35 | <0.001* |
| pTb.Th (mm) | 0.14 ± 0.02 | 0.13 ± 0.01[b] | 0.15 ± 0.02 | 0.01 |
| rTb.Th (mm) | 0.09 ± 0.01[a] | 0.09 ± 0.01[b] | 0.12 ± 0.02 | <0.001 |
| pTb.S (mm2) | 0.05±0[a] | 0.06 ± 0.01[b] | 0.09 ± 0.03 | <0.001 |
| rTb.l (mm) | 0.33 ± 0.02[a] | 0.33 ± 0.04[b] | 0.42 ± 0.08 | <0.001 |
| R–R Junc.D (1/mm3) | 7.56 ± 4.46[a] | 4.79 ± 3.72 | 3.17 ± 1.7 | 0.03 |
| R–P Junc.D (1/mm3) | 45.37 ± 24.68[a] | 17.63 ± 10.02 | 15.59 ± 11.26 | <0.001* |
| P–P Junc.D (1/mm3) | 31.67 ± 12.81[a] | 14.89 ± 6.57 | 13.93 ± 10.89 | <0.001* |
| **μFEA** | | | | |
| Stiffness (kN/mm) | 12003.56 ± 7590.42 | 4964.01 ± 3778.37 | 5908.58 ± 5029.27 | 0.013* |
| Failure Load (MPa) | 477.7 ± 279.56 | 215.89 ± 143.73 | 229.76 ± 200.91 | 0.013* |

Values represent mean ± SD.
a = axial; BV = bone volume; Conn.D = connenctivity density; CT = computed tomography; ITS = ; NC = normal control; OA = osteoarthritis; OP = osteoporosis. p = plate; P–P Junc.D = plate–plate junction density; r = rod; R–P Junc.D = rod–plate junction density; R–R Junc.D = rod–rod junction density; SMI = structure model index; Tb.l = trabecular length; Tb.N = trabecular number; Tb.S = trabecular surface area; Tb.Sp = trabecular separation; Tb.Th = trabecular thickness; TV = total volume.
*$p < 0.05$ between OA and OP group and remained significant after adjustment for age and weight.
[a] p<0.05 between OA and NC groupand and remained significant after adjustment for age and weight.
[b] $p < 0.05$ between OP and NC groupand and remained significant after adjustment for age and weight.

in paraffin. We obtained 5 mm-thick sagittal-oriented sections and processed them for safranin O/fast green and haematoxylin and eosin (H&E) staining. Cartilage degeneration of the histological sections was assessed using Osteoarthritis Research Society International (OARSI) scores [33, 34]. The grade and stage of the femur cartilage were assessed by a blinded technician. The OARSI score was calculated by multiplying the grade and stage values for each section, with the score ranging from 0 (i.e., no OA activity) to 24 (i.e., heaviest degree of OA).

### *Statistical analysis*

All variables were presented as mean ± SD. Clinical variables, body measurements, trabecular microstructure parameters, μFEA parameters, and OARSI scores were evaluated using independent one-way analysis of variance for comparisons between the three groups and using the two-sided Student's t tests for comparisons between two groups. Age and weight ($p < 0.05$ for both, independent from each other) were selected as covariates for multiple linear regression analysis. Pearson analysis was applied to analyse the relationships between bone microstructure and mechanical indicators. For all analyses, two-tailed values of $p < 0.05$ were considered statistically significant. All statistical analyses were performed using SPSS 22.0 software (SPSS Inc., Chicago, IL, USA).

## Results

Patients in the OA group were heavier (mean weight: 63.23 ± 11.1 kg vs 54.24 ± 9.31 kg, $p < 0.05$) and younger (mean age, 52.31 ± 13.39 years vs and 75.71 ± 9.82 years, $p < 0.05$) than those in the OP group, while there was no significant difference in height (mean height, 163.38 ± 7.57 cm vs 160.12 ± 6.18 cm, $p = 0.31$) between the two groups. The mean patient age in the NC group was 65.25 ± 23.3 years; mean height, 164.63 ± 6.76 cm; and mean weight, 65.13 ± 3.83 kg. The patient characteristics are detailed in Table 1. Bone mineral density, as well as the T value, in the hip and lumbar regions was significantly lower in the OP group than those in the OA and NC groups ($p < 0.05$). The OARSI score was significantly higher in the OA group than that in the OP and NC groups ($p < 0.05$).

For the H&E and safranin O/fast green staining (Fig. 2), the cartilage in the OA group showed serious damage, and the OARSI score was the highest in the OA group followed by that in the OP group ($p < 0.05$). For the standard and ITS-based bone microstructure (Table 2), the OA group had more Tb.N (61%), Conn. D (108%), pTb.N (27%), rTb.N (34%), R–R Junc. D (138%), R–P Junc. D (191%), P–P Junc. D (127%) and less rTb.Th (25%), pTb.S (44%), and rTbl (21%) than did the NC group ($p < 0.05$). The OP group had less pTb.Th (13%), rTb.Th (25%), pTb.S (33%), and rTb.l (21%) than the NC group ($p < 0.05$). The OA group had more BV/TV (91%), Tb.N (96%), Conn. D (125%), pBV/TV (137%), rBV/TV (70%), pTb.N (24%), rTb.N (26%), R–P Junc. D (157%), and P–P Junc. D (113%) and less Tb. Sp (38%) than did the OP group ($p < 0.05$). For the mechanical properties detected via μFEA, the OA group had higher stiffness (142%) and failure load (121%) than did the OP group ($p < 0.05$). For all the samples (n = 38, Table 3), both the stiffness and the failure load was positively correlated with BV/TV, Tb.N, Tb.Th, Conn. D, aBV/TV, pBV/TV, rBV/TV, pTb.N, rTb.N, pTbTh, R–R Junc. D, R–P JuncD, and P–P JuncD and negatively correlated with Tb. Sp and SMI ($p < 0.05$).

The relationship varied when divided according to the disease (Table 4). In the OA group, both the stiffness and the failure load were positively correlated with BV/TV, TbN, Tb.Th, Conn. D, aBV/TV, pBV/TV, rBV/TV, pTb.N, rTb.N, pTbTh, rTb.l, R–R Junc. D, R–P JuncD, and P–P JuncD and negatively corelated with Tb. Sp and SMI ($p < 0.05$). In the OP group, both the stiffness and the failure load were positively correlated with BV/TV, TbN, Tb.Th, SMI, aBV/TV, pBV/TV, pTb.N, pTbTh, R–P JuncD (except for failure load), and P–P JuncD ($p < 0.05$). In the NC group, both the stiffness and the failure load were positively correlated with BV/TV, aBV/TV, pBV/TV, pTb.N, R–P JuncD, and P–P

**Table 3**
Correlation coefficient of linear regression between the subchondral microstructure and biomechanical properties in the all 3 groups.

| Microstructure | ALL (n = 38) | |
|---|---|---|
| | Stiffness | Failure Load |
| **Standard micro-CT** | | |
| BV/TV (%) | 0.92** | 0.91** |
| Tb.N (1/mm) | 0.73** | 0.71** |
| Tb.Th (mm) | 0.71** | 0.71** |
| Tb.Sp | −0.68** | −0.66** |
| SMI | −0.81** | −0.79** |
| Conn.D (1/mm3) | 0.60** | 0.59** |
| **ITS-based micro-CT** | | |
| aBV/TV (%) | 0.93** | 0.91** |
| pBV/TV (%) | 0.93** | 0.91** |
| rBV/TV (%) | 0.63** | 0.63** |
| pTb.N (1/mm) | 0.80** | 0.79** |
| rTb.N (1/mm) | 0.68** | 0.67** |
| pTb.Th (mm) | 0.50** | 0.47** |
| rTb.Th (mm) | −0.24 | −0.27 |
| pTb.S (mm2) | −0.22 | −0.24 |
| rTb.l (mm) | −0.14 | −0.16 |
| R–R Junc.D (1/mm3) | 0.46** | 0.47** |
| R–P Junc.D (1/mm3) | 0.87** | 0.87** |
| P–P Junc.D (1/mm3) | 0.84** | 0.83** |
| **μFEA** | | |
| Stiffness (kN/mm) | 1 | 0.99** |
| Failure Load (MPa) | 0.99** | 1 |
| OARSI | 0.32 | 0.33* |

*p < 0.05.
**p < 0.01.

JuncD and negatively correlated with SMI, rTb.Th, and rTb.l ($p < 0.05$).

## Discussion

This study used ITS to compare differences in the plate and rod microstructure and evaluate the variations in mechanical property between OA and OP. The results showed that the plate and rod microstructures change differently in OA than those in OP. OA gained more plate and rTb.N, while OP lost more pTbTh compared with the NC group. OA had better mechanical properties and more structure parameters such as rBV/TV and rTb.N that were positively correlated with such properties than OP. These microstructure differences may help explain the variation in mechanical properties among different bone diseases, particularly between OP and OA.

Animals models showed transient bone loss in the subchondral bone in the early stages of OA [35]. Ding et al. [36] found a thicker and more plate-like trabecular bone structure of the tibial plateau in early OA. In advanced OA, the subchondral bone may have sclerosis due to abnormal bone remodelling accompanied by reduced mineralisation [13,18,37,38]. In our study, the OA group had more Tb.N, Conn. D, pTb.N, rTb.N, R–R Junc. D, R–P Junc. D, and P–P Junc. D and less rTb.Th, pTb.S, rTbl than did the NC group. These findings indicate that the change of the plate–rod structure in the subchondral bone is crucial in the development of OA. Using bone histomorphometry, Bobinac et al. [39] found subchondral changes in tibial plateau from knee OA patients. The BV/TV was higher, while the Tb.N was lower in the lateral condyle. Chen et al. [40] studied the tibial plateau of the OA patients and observed rTb.N loss. They also noted thickening of both pTb.Th and rTb.Th in the advanced OA group regardless of cartilage structure (damaged or intact). In contrast, we found that pTb.N increased with cartilage damage in the OA group. Such difference may be due to the differences in the studied locations [41]. Shimamura et al. [42] found no changes in Tb.Th in the femoral head subchondral bone in patients with end-stage hip OA. Further, compared with the intact cartilage area, the Tb.N was increased in the damaged cartilage area, which may be related to the changes in the subchondral plate [15,26]. In addition, the abnormal load bearing may increase the bone volume by remodelling in the hip joint [43,44]. Meanwhile, in contrast the findings of previous studies [35,36,39], we did not observe a significant change in SMI between the OA and the

**Table 4**
Correlation coefficient of linear regression between the subchondral microstructure and biomechanical properties in the OA, OP and NC groups.

| Microstructure | OA (n = 13) | | OP (n = 17) | | NC (n = 8) | |
|---|---|---|---|---|---|---|
| | Stiffness | Failure Load | Stiffness | Failure Load | Stiffness | Failure Load |
| **Standard micro-CT** | | | | | | |
| BV/TV (%) | 0.95** | 0.98** | 0.89** | 0.86** | 0.84** | 0.74* |
| Tb.N (1/mm) | 0.92** | 0.93** | 0.56* | 0.52* | 0.58 | 0.46 |
| Tb.Th (mm) | 0.67* | 0.69** | 0.69** | 0.68** | 0.65 | 0.65 |
| Tb.Sp | −0.83** | −0.85** | −0.48 | −0.46 | −0.28 | −0.17 |
| SMI | −0.89** | −0.91** | −0.90** | −0.91** | −0.92** | −0.88** |
| Conn.D (1/mm3) | 0.82** | 0.85** | 0.29 | 0.24 | 0.38 | 0.26 |
| **ITS-based micro-CT** | | | | | | |
| aBV/TV (%) | 0.98** | 0.97** | 0.90** | 0.87** | 0.90** | 0.84** |
| pBV/TV (%) | 0.96** | 0.97** | 0.87** | 0.84** | 0.92** | 0.84** |
| rBV/TV (%) | 0.80** | 0.85** | 0.17 | 0.15 | −0.57 | −0.6 |
| pTb.N (1/mm) | 0.82** | 0.83** | 0.58* | 0.53* | 0.87** | 0.82* |
| rTb.N (1/mm) | 0.86** | 0.88** | 0.08 | 0.04 | 0.55 | 0.47 |
| pTb.Th (mm) | 0.88** | 0.88** | 0.70** | 0.68** | −0.34 | −0.34 |
| rTb.Th (mm) | 0.31 | 0.37 | 0.13 | 0.16 | −0.91** | −0.91** |
| pTb.S (mm2) | 0.37 | 0.36 | 0.36 | 0.39 | −0.62 | −0.61 |
| rTb.l (mm) | 0.66* | 0.71** | 0.09 | 0.14 | −0.89** | −0.88** |
| R–R Junc.D (1/mm3) | 0.67* | 0.72** | −0.18 | −0.21 | 0.24 | 0.15 |
| R–P Junc.D (1/mm3) | 0.95** | 0.96** | 0.50* | 0.44 | 0.78* | 0.68 |
| P–P Junc.D (1/mm3) | 0.87** | 0.88** | 0.54* | 0.49* | 0.79* | 0.71 |
| **μFEA** | | | | | | |
| Stiffness (kN/mm) | 1 | 0.987** | 1 | 1** | 1 | 0.98** |
| Failure Load (MPa) | 0.99** | 1 | 1** | 1 | 0.98** | 1 |
| OARSI | −0.29 | −0.24 | −0.22 | −0.22 | −0.33 | −0.42 |

*p < 0.05.
**p < 0.01.
a = axial; BV = bone volume; Conn.D = connenctivity density; CT = computed tomography; ITS = ; NC = normal control; OA = osteoarthritis; OP = osteoporosis. p = plate; P–P Junc.D = plate–plate junction density; r = rod; R–P Junc.D = rod–plate junction density; R–R Junc.D = rod–rod junction density; SMI = structure model index; Tb.l = trabecular length; Tb.N = trabecular number; Tb.S = trabecular surface area; Tb.Sp = trabecular separation; Tb.Th = trabecular thickness; TV = total volume.

control group, which may be due to the small sample size.

In our study, both the plate, rod, and conventional bone volume fraction and number were higher in the OA group than those in the OP group. The OA group had higher stiffness and failure load than did the OP group, whereas there was no significant intergroup difference in thickness. Zhang et al. observed that, among postmenopausal women, those with OA had higher bone microstructural indicators such as BV/TV, Tb.N, and Tb.Th than those with OP as assessed via histomorphometry [45]. Higher BV/TV and Tb.Th as assessed via μCT were also noted [18,19]. The difference in thickness was discussed as follows. In their study, the distribution of the rod and plate in the microstructure was evaluated using SMI, where an increased plate-like structure was observed. R–P and P–P Junc. D values were significantly higher in the OA group than those in the OP group. In contrast, R–R did not differ between the two groups. This may be due to the lesser Tb. Sp and richer trabecular mesh network of OA and is consistent with the findings of a previous study [46]. Liu et al. studied premenopausal women with idiopathic osteoporosis and found a more rod-like trabecular microstructure in the distal radius, but not in the distal tibia [24]. In our study, the OP group had less pTb.Th, rTb.Th, pTb.S, and rTb.l than the NC group, which may be due to the different locations and the limited sample size in our study, as we only studied the femoral heads.

While examining the mechanical properties of the subchondral bone, we found that both stiffness and failure load were significantly higher in the OA group than in the OP group, showing that OA might have better mechanical properties than OP. Zhang et al. found that all four mechanical parameters (i.e., Young's modulus, compressive strength, yield strength, and maximum compressive force) were higher in the OA group than in the OP group [19]. Li et al. also found that ultimate stress and the elastic modulus were higher in the OA group than those in the OP group [18]. Previous studies showed that BV/TV is an important indicator reflecting bone strength and is positively associated with mechanical properties [47,48]. However, we found that different types of trabecular bone in the three groups have different effects on mechanical properties. Among these structure–function indicators, we found that the plate structure such as pBV/TV, pTb.N, R–P JuncD, and P–P JuncD were positively correlated with the mechanical strength in all three groups. Meanwhile, rBV/TV, rTb.N, and R–R Junc. D were not linearly related to stiffness or failure load in the OP and NC groups. In contrast, the SMI, rTb.Th, and rTb.l were negatively correlated to the stiffness and the failure load in the NC group. This is consistent with former ITS studies that showed that the plate structure has more profound effect on the mechanical property, while rod structure has little effect on the change of the mechanical properties [23,27,46]. As for the differences in structure–function relationship between OA and other bone disease it may be related with the bone cysts in OA subchondral bone. In OA, cysts were widely distributed and were related with BV/TV. Further, they had a negative impact on mechanical property [49] and mineralisation [50]. However, As this is a cross-sectional study, we cannot investigate the casual relationship between the microstructure and mechanical strength. Nonetheless, it can be inferred that in OA, both plate and rod microstructure (number and junction density) in the trabecular bone synchronised at the late stage. This enhanced the relationship between the rod microstructure and the mechanical property, consistent with previous research [18]. The OP trabecular bone lost both plate and rod microstructure (thickness and length), which may weaken mechanical properties.

There are several limitations associated with this study. First, its sample size was small, but we used strict inclusion criteria and excluded any OA patient with OP symptoms. Second, we did not collect data on possible biochemical indicators such as the parathyroid hormone level and serum calcium level. Third, our study did not include patients with early lesions because of the use of *ex vivo* specimens. Previous studies showed that there may be no distinct microstructural changes in early stage OA. Fourth, due to the small sample size, we did not divide the patients by sex, which may influence results. Despite these limitations, our study is valuable in that we identified the differences in plate and rod microstructures between OA and OP and investigated their influence on mechanical property. Further research is needed to investigate the significance of subchondral bone microstructural changes in disease diagnosis and treatment.

In conclusion, we found distinctive features in the subchondral trabecular bone between OA and OP. OA had more plate and rod microstructures, and these microstructures exerted a more profound influence on mechanical strength in OA than in OP. These differences may help explain the variation of mechanical properties among these bone diseases.

## Funding

This work was supported by grants from the National Natural Science Foundation of China [grant numbers 11572197 and 11872251].

## Conflict of Interest

The authors have no conflicts of interest to disclose in relation to this article.

## Acknowledgements

The authors thank the patients in this study and the participating surgeon who contributed in the data collection.

## References

[1] Chu CR, Millis MB, Olson SA. Osteoarthritis: from palliation to prevention: AOA critical issues. J Bone Jt Surg Am 2014;96(15):e130.
[2] Fahlman L, Sangeorzan E, Chheda N. Older subjects without radiographic knee osteoarthritis: weight, height, and body mass index. Aging and disease 2013;4(4):201–9 [eng].
[3] Consensus development conference: prophylaxis and treatment of osteoporosis. Osteoporos Int 1991;1(2):114–7 [eng].
[4] Lorentzon M, Cummings SR. Osteoporosis: the evolution of a diagnosis. J Intern Med 2015;277(6):650–61.
[5] Hart DJ, Mootoosamy I, Doyle DV, Spector TD. The relationship between osteoarthritis and osteoporosis in the general population: the Chingford Study. Ann Rheum Dis 1994;53(3):158–62.
[6] Healey JH, Vigorita VJ, Lane JM. The coexistence and characteristics of osteoarthritis and osteoporosis. J Bone Joint Surg Am 1985;67(4):586–92 [eng].
[7] Antoniades L, MacGregor AJ, Andrew T, Spector TD. Association of birth weight with osteoporosis and osteoarthritis in adult twins. Rheumatology 2003;42(6):791–6 [eng].
[8] Glowacki J, Hurwitz S, Thornhill TS, Michael K, Meryl SL. Osteoporosis and vitamin-D deficiency among postmenopausal women with osteoarthritis undergoing total hip arthroplasty. J Bone Jt Surg Am 2003;85–A(12):2371.
[9] Shen Y, Zhang Y-H, Shen L. Postmenopausal women with osteoporosis and osteoarthritis show different microstructural characteristics of trabecular bone in proximal tibia using high-resolution magnetic resonance imaging at 3 tesla. BMC Muscoskel Disord 2013;14(1):136.
[10] Bobinac D, Marinovic M, Bazdulj E, Cvijanovic O, Celic T, Maric I, et al. Microstructural alterations of femoral head articular cartilage and subchondral bone in osteoarthritis and osteoporosis. Osteoarthritis Cartilage 2013;21(11):1724–30 [eng].
[11] Buckland-Wright C. Subchondral bone changes in hand and knee osteoarthritis detected by radiography. Osteoarthritis Cartilage 2004;12:10–9.
[12] Madry H. The subchondral bone: a new frontier in articular cartilage repair. Knee Surg Sports Traumatol Arthrosc : off J ESSKA 2010;18(4):417–8 [eng].
[13] Li G, Yin J, Gao J, Cheng TS, Pavlos NJ, Zhang CQ, et al. Subchondral bone in osteoarthritis: insight into risk factors and microstructural changes. Arthritis Res Ther 2013;15(6):223 [eng].
[14] Li B, Aspden RM. Composition and mechanical properties of cancellous bone from the femoral head of patients with osteoporosis or osteoarthritis. J Bone Miner Res 1997;12(4):641–51 [eng].
[15] Burr DB, Gallant MA. Bone remodelling in osteoarthritis. Nat Rev Rheumatol 2012;8(11):665–73.
[16] Castañeda S, Romanblas JA, Largo R, Herrero G. Subchondral bone as a key target for osteoarthritis treatment. Biochem Pharmacol 2012;83(3):315–23.
[17] Chiba K, Uetani M, Kido Y, Ito M, Okazaki N, Taguchi K, et al. Osteoporotic changes of subchondral trabecular bone in osteoarthritis of the knee: a 3-T MRI study. Osteoporos Int 2012;23(2):589–97.
[18] Li ZC, Dai LY, Jiang LS, Qiu SJ. Difference in subchondral cancellous bone between postmenopausal women with hip osteoarthritis and osteoporotic fracture:

implication for fatigue microdamage, bone microarchitecture, and biomechanical properties. Arthritis Rheum 2012;64(12):3955–62.
[19] Zhang Z-M, Li Z-C, Jiang L-S, Jiang S-D, Dai L-Y. Micro-CT and mechanical evaluation of subchondral trabecular bone structure between postmenopausal women with osteoarthritis and osteoporosis. Osteoporos Int 2010;21(8):1383–90.
[20] Eastell R, Szulc P. Use of bone turnover markers in postmenopausal osteoporosis. Lancet Diabetes Endocrinol 2017;5(11):908–23 [eng].
[21] Rogers A, Hannon RA, Eastell R. Biochemical markers as predictors of rates of bone loss after menopause. J Bone Miner Res 2000;15(7):1398–404 [eng].
[22] Resmini G, Migliaccio S, Dalle Carbonare L, Sala U, Brama M, Fornari R, et al. Differential characteristics of bone quality and bone turnover biochemical markers in patients with hip fragility fractures and hip osteoarthritis: results of a clinical pilot study. Aging Clin Exp Res 2011;23(2):99–105 [eng].
[23] Liu XS, Sajda P, Saha PK, Wehrli FW, Bevill G, Keaveny TM, et al. Complete volumetric decomposition of individual trabecular plates and rods and its morphological correlations with anisotropic elastic moduli in human trabecular bone. J Bone Miner Res 2008;23(2):223–35 [eng].
[24] Liu XS, Cohen A, Shane E, Stein E, Rogers H, Kokolus SL, et al. Individual trabeculae segmentation (ITS)-based morphological analysis of high-resolution peripheral quantitative computed tomography images detects abnormal trabecular plate and rod microarchitecture in premenopausal women with idiopathic osteoporosis. J Bone Miner Res 2010;25(7):1496–505 [eng].
[25] Altman R, Alarcon G, Appelrouth D, Bloch D, Borenstein D, Brandt K, et al. The American College of Rheumatology criteria for the classification and reporting of osteoarthritis of the hip. Arthritis Rheum 1991;34(5):505–14 [eng].
[26] Chu LY, He ZH, Qu XH, Liu XQ, Zhang WT, Zhang S, et al. Different subchondral trabecular bone microstructure and biomechanical properties between developmental dysplasia of the hip and primary osteoarthritis. J Orthopaedic Translation 2019;22:50–7.
[27] Liu XS, Sajda P, Saha PK, Wehrli FW, Guo XE. Quantification of the roles of trabecular microarchitecture and trabecular type in determining the elastic modulus of human trabecular bone. J Bone Miner Res 2006;21(10):1608–17.
[28] Liu XS, Bevill G, Keaveny TM, Sajda P, Guo XE. Micromechanical analyses of vertebral trabecular bone based on individual trabeculae segmentation of plates and rods. J Biomech 2009;42(3):249–56 [eng].
[29] Liu XS, Walker MD, McMahon DJ, Udesky J, Liu G, Bilezikian JP, et al. Better skeletal microstructure confers greater mechanical advantages in Chinese-American women versus white women. J Bone Miner Res 2011;26(8):1783–92.
[30] Van Rietbergen B, Odgaard A, Kabel J, Huiskes R. Direct mechanics assessment of elastic symmetries and properties of trabecular bone architecture. J Biomech 1996;29(12):1653–7 [eng].
[31] Wang J, Zhou B, Liu XS, Fields AJ, Sanyal A, Shi XT, et al. Trabecular plates and rods determine elastic modulus and yield strength of human trabecular bone. Bone 2015;72:71–80 [eng].
[32] van Lenthe GH, Müller R. Prediction of failure load using micro-finite element analysis models: toward in vivo strength assessment. Drug Discov Today Technol 2006;3(2):221–9.
[33] Waldstein W, Perino G, Gilbert SL, Maher SA, Windhager R, Boettner F. OARSI osteoarthritis cartilage histopathology assessment system: a biomechanical evaluation in the human knee. J Orthop Res 2016;34(1):135–40.
[34] Pritzker KP, Gay S, Jimenez SA, Ostergaard K, Pelletier JP, Revell PA, et al. Osteoarthritis cartilage histopathology: grading and staging. Osteoarthritis Cartilage 2006;14(1):13–29 [eng].
[35] Ding M, Danielsen CC, Hvid I. Age-related three-dimensional microarchitectural adaptations of subchondral bone tissues in Guinea pig primary osteoarthrosis. Calcif Tissue Int 2006;78(2):113–22.
[36] Ding M, Odgaard A, Hvid I. Changes in the three-dimensional microstructure of human tibial cancellous bone in early osteoarthritis. J Bone Joint Surg British 2003;85(6):906–12 [eng].
[37] Goldring SR, Goldring MB. Changes in the osteochondral unit during osteoarthritis: structure, function and cartilage-bone crosstalk. Nat Rev Rheumatol 2016;12(11):632–44 [eng].
[38] Madry H, Van Dijk CN, Muellergerbl M. The basic science of the subchondral bone. Knee Surg Sports Traumatol Arthrosc 2010;18(4):419–33.
[39] Bobinac D, Spanjol J, Zoricic S, Maric I. Changes in articular cartilage and subchondral bone histomorphometry in osteoarthritic knee joints in humans. Bone 2003;32(3):284–90.
[40] Yan C, Yizhong H, Eric YY, Zhang XJ, Watts T, Zhou B, et al. Subchondral trabecular rod loss and plate thickening in the development of osteoarthritis. J Bone Miner Res 2018;33(2):316–27.
[41] Kroker A, Bhatla JL, Emery CA, Manske SL, Boyd SK. Subchondral bone microarchitecture in ACL reconstructed knees of young women: a comparison with contralateral and uninjured control knees. Bone 2018;111:1–8.
[42] Shimamura M, Iwata K, Mashiba T, Miki T, Yamamoto T. Accumulation of microdamage in subchondral bone at the femoral head in patients with end-stage osteoarthritis of the hip. J Bone Miner Metabol 2019;37(5):880–5.
[43] Cox LGE, van Donkelaar CC, van Rietbergen B, Emans PJ, Ito K. Decreased bone tissue mineralization can partly explain subchondral sclerosis observed in osteoarthritis. Bone 2012;50(5):1152–61.
[44] Li G, Ma Y, Cheng TS, Landao-Bassonga E, Qin A, Pavlos NJ, et al. Identical subchondral bone microarchitecture pattern with increased bone resorption in rheumatoid arthritis as compared to osteoarthritis. Osteoarthritis Cartilage 2014;22(12):2083–92.
[45] Zhang Z, Jiang L, Jiang S, Dai LY. Differential articular calcified cartilage and subchondral bone in postmenopausal women with osteoarthritis and osteoporosis: two-dimensional analysis. Joint Bone Spine 2009;76(6):674–9.
[46] Liu SX, Shane E, McMahon DJ, Guo XE. Individual trabecula segmentation (ITS)–based morphological analysis of microscale images of human tibial trabecular bone at limited spatial resolution. J Bone Miner Res 2011;26(9):2184–93.
[47] Karim L, Vashishth D. The role of trabecular microarchitecture in the formation, accumulation, and morphology of microdamage in human cancellous bone. J Orthop Res 2011;29(11):1739–44.
[48] Hui SL, Slemenda CW, Johnston CC. Age and bone mass as predictors of fracture in a prospective study. J Clin Invest 1988;81(6):1804–9.
[49] Chiba K, Burghardt AJ, Osaki M, Majumdar S. Three-dimensional analysis of subchondral cysts in hip osteoarthritis: an ex vivo HR-pQCT study. Bone 2014;66:140–5 [eng].
[50] Chiba K, Nango N, Kubota S, Okazaki N, Taguchi K, Osaki M, et al. Relationship between microstructure and degree of mineralization in subchondral bone of osteoarthritis: a synchrotron radiation μCT study. J Bone Miner Res 2012;27(7):1511–7.